Mineralizer-Assisted Shape-Control of Rare Earth Oxide Nanoplates

ARTICLE *in* CHEMISTRY OF MATERIALS · SEPTEMBER 2014

Impact Factor: 8.35 · DOI: 10.1021/cm502301u

CHEMISTRY OF MATERIALS

Article

pubs.acs.org/cm

Mineralizer-Assisted Shape-Control of Rare Earth Oxide Nanoplates

Dianyuan Wang,[†,‡,⊥] Yijin Kang,[‡,⊥,¶] Xingchen Ye,[‡,∥] and Christopher B. Murray*[,‡,§]

[†]College of Science, Jiujiang University, Jiujiang 332005, P. R. China

[‡]Department of Chemistry and [§]Department of Materials Science and Engineering, University of Pennsylvania, Philadelphia, Pennsylvania 19104, United States

Supporting Information

ABSTRACT: Rare earth oxides are important emerging materials because of their unique properties. Nanosized, two-dimentional (2D) materials have received increasing attention due to their high surface-to-volume ratios and ultrathin layered structures. Here, we synthesize 2D rare earth (RE) oxide nanoplates in the presence of a mineralizer. The use of a mineralizer not only facilitates the synthesis of RE oxide nanoplates (i.e., increases the yield and allows mild reaction parameters), but also allows for shape-control. To emphasize the importance of RE oxide nanoplates in materials science and engineering, we demonstrate that (1) ceria nanoplates can be used in a ceria/Cu inverse catalyst to enable an enhanced CO oxidation activity, and (2) Y_2O_3 nanoplates doped with Eu^{3+} enable photon energy down-conversion.

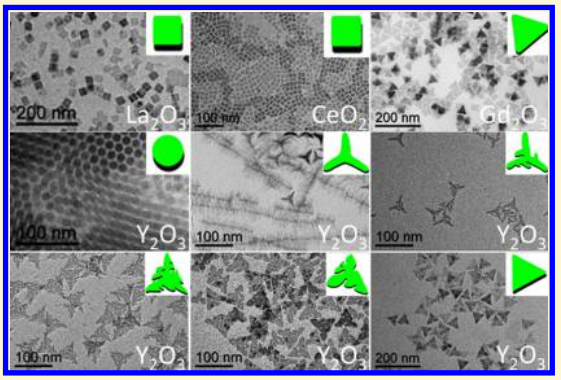

The synthesis and preparation of nanomaterials are the foundations of nanoscience and nanotechnology.[1,2] The shape-controlled synthesis of nanomaterials is of particular interest, because the properties of nanomaterials can be fine-tuned by tailoring the shape of the nanomaterials, which enables the application of nanomaterials in various fields, such as catalysis,[3−20] electronics,[21] optics,[22−25] magnetics,[26] etc.[27]

Rare earth (RE) compound nanomaterials are an emerging class of nanomaterials because of their special properties.[28] For instance, ceria nanomaterials are widely applied in catalysis because they can store and carry oxygen because of the easy conversion between Ce^{3+} and Ce^{4+}.[18,29] Lanthanide-doped nanophosphors (e.g., β-$NaYF_4$, Y_2O_3) possess intriguing optical properties such as photon upconversion or downconversion.[23,30] Among these materials, ultrathin two-dimensional (2D) nanomaterials such as nanoplates are particularly attractive, mainly because of their high surface-to-volume ratios.[18,23,31−36] The thickness of a 2D nanostructure could be as thin as ∼2 nm, which is in the order of only a few atomic layers.[18,31] Many interesting properties arise from such high surface-to-volume ratios and the ultrathin layered structures. For instance, compared to three-dimensional (3D) Ceria nanoparticles, 2D ceria nanoplates allow oxygen to easily diffuse into their bodies, and thus do not limit the oxygen storage at the surface of ceria materials.[18] In the doped phosphors, the dopant element may readily enter the body of the host-materials, which thus maximizes the efficiency.[23] Additionally, the confininement on the plates may add a potential quantum size effect.[36] Because of the importance of 2D RE materials, numerous synthetic methods and preparation routes were developed, including hydrothermal treatment,[37] chemical vapor deposition,[38] and solution-phase-synthesis.[18,23] In a previous report we demonstrated a robust solution-phase-synthesis of ultrathin 2D ceria nanoplates using a mineralizer.[18] The presence of the mineralizer not only allows mild reaction conditions, but also significantly improves the yield and quality of 2D nanoplates.[18]

Here we report a systematic study of mineralizer-assisted shape-control of rare earth (RE) oxide (RE = La, Ce, Gd, Y) nanoplates. Examples of the four selected RE elements are presented: La and Ce are light RE elements; Y is a heavy RE element; and Gd is on the boundary, that is, the "heaviest" light RE element.[39] We also demonstrate the benefits gained from the 2D structure with one case of highly efficient ceria nanoplate/Cu dendrite inverse catalysts for CO oxidation and one case of optical downconversion by 2D Eu^{3+}-doped Y_2O_3 nanophosphors.

RESULTS AND DISCUSSION

The synthesis of RE oxide nanoplates involves the thermal decomposition of RE acetate at 320−330 °C in the presence of oleic acid and oleylamine as stabilizers and employs sodium diphosphate or sodium nitrate as mineralizers. With the mineralizers, the yields of RE oxide nanoplates is significantly improved (Table S1, Supporting Information). Most importantly, the morphology of the nanoplates can be readily tuned by the manipulation of the reaction conditions, such as the reaction temperature, precursor/ligands ratio, etc. In contrast, such morphology control cannot be achieved in the absence of mineralizers. The transmission electron microscopy (TEM) images of typical RE oxide nanoplates synthesized in the

Received: June 25, 2014
Revised: August 25, 2014

   dx.doi.org/10.1021/cm502301u | Chem. Mater. XXXX, XXX, XXX−XXX

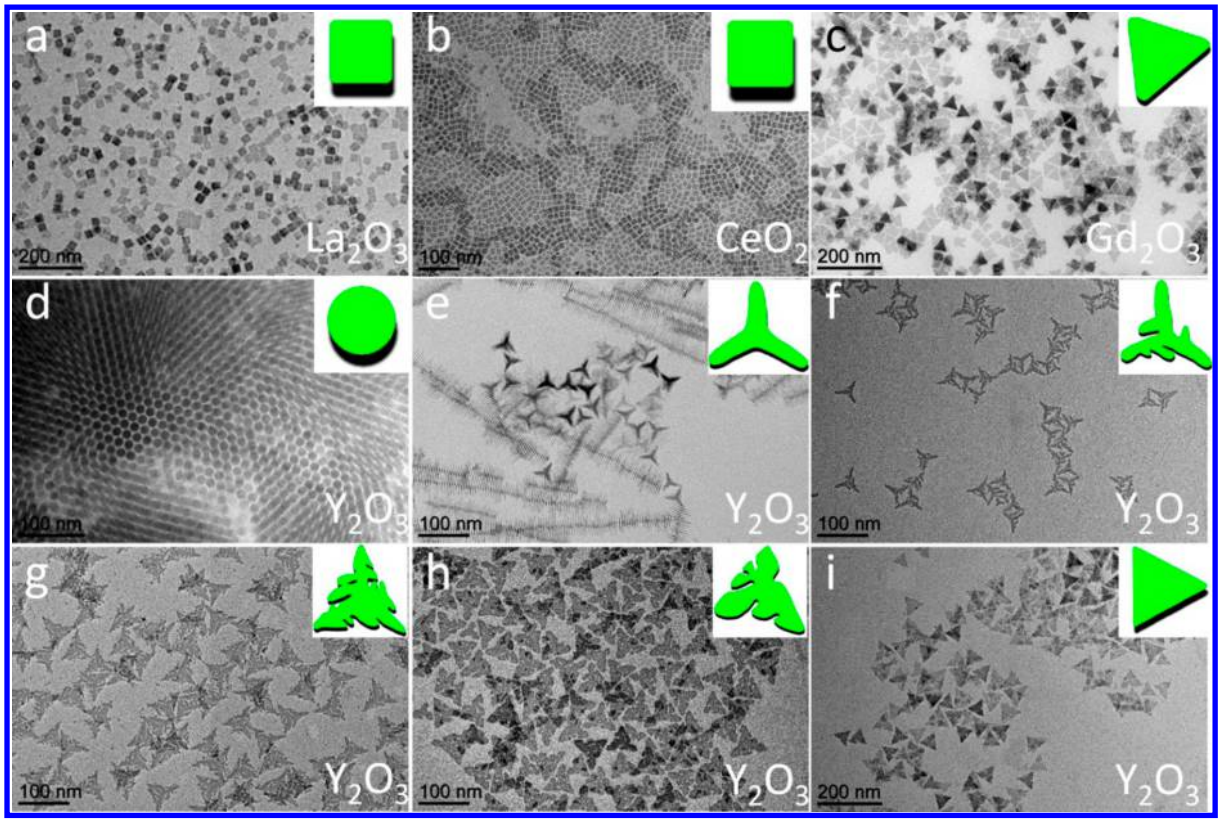

Figure 1. TEM images of (a) 25.2 nm (σ = 7%) La_2O_3 nanoplates; (b) 11.9 nm (σ = 7%) CeO_2 nanoplates; (c) 39.4 nm (σ = 6%) Gd_2O_3 nanoplates; and (d) 13.6 nm (σ < 5%), (e) 36.7 nm (σ = 6%), (f) 43.7 nm (σ = 8%), (g) 58.6 nm (σ = 7%), (h) 62.7 nm (σ = 7%), and (i) 56.9 nm (σ = 9%) Y_2O_3 nanoplates. Scale bars: 200 nm (a, c, and i) and 100 nm (b, d, e, f, g, and h).

presence of mineralizers are exhibited in Figure 1. As shown in Figure 1, panel a, the La_2O_3 square nanoplates with edge lengths of 25.2 nm (σ = 7%) are synthesized in the presence of sodium diphosphate, while no nanoplates are generated in the absence of the mineralizers. Similarly, the square ceria nanoplates with edge lengths of 11.9 nm (σ = 7%) can be obtained using sodium diphosphate as a mineralizer (Figure 1b), while the reaction without the mineralizer does not produce any ceria nanoplates. In our previous report, we showed that elongated ceria nanoplates can be synthesized with sodium oleate as the mineralizer.[18] For Gd_2O_3, in addition to square and round nanoplates, triangular nanoplates with edge lengths of 39.4 nm (σ = 6%) are synthesized using sodium nitrate as the mineralizer (Figure 1c). Y_2O_3 has the greatest range of morphologies: without any mineralizer, round nanoplates are produced; in the presence of sodium diphosphate, highly monodisperse round nanoplates with diameters of 13.6 nm (σ < 5%) are generated; with sodium nitrate, the shape of the Y_2O_3 nanoplates are tuned from tripods (Figure 1e: 36.7 nm, σ = 6%) and branched tripods (Figure 1f: 43.7 nm, σ = 8%) to triangular nanoplates (Figure 1i: 56.9 nm, σ = 9%) by increasing the amount of oleylamine in the reactions. The transition between tripod and triangular nanoplates can be fine-tuned by manipulating the reaction parameters, such as the precursor concentration and the mineralizer concentration. For instance, a reduction of the precursor concentration by a factor of two synthesizes the highly branched tripods (58.6 nm, σ = 7%); when the concentration of sodium nitrate is doubled, the almost complete transformation into triangular nanoplates (62.7 nm, σ = 7%) is observed (Figure S1, Supporting Information).

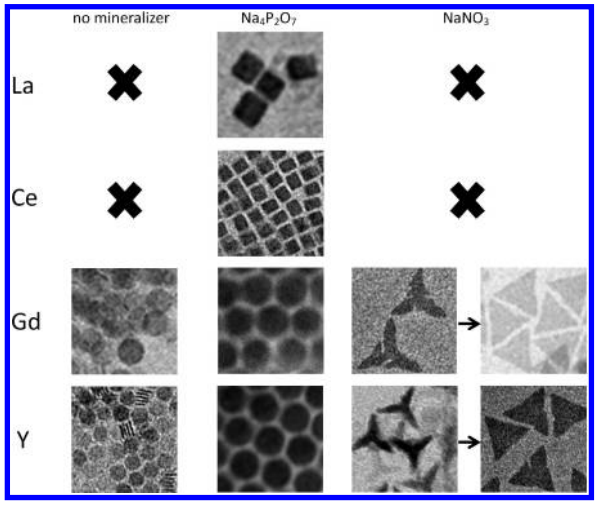

Figure 2. Chart that shows the correlation between the obtained morphologies of RE oxide nanoplates and the mineralizers used in the synthesis. The dimensions of the TEM images are 100 nm × 100 nm.

The mineralizers play an important role in the synthesis of RE oxide nanoplates. As summarized in Figure 2 and Table S1 of the Supporting Information, the yield of nanoplates is significantly increased by the use of mineralizers. More importantly, in some cases (e.g., in light RE elements such as La and Ce), nanoplates cannot be produced without the employment of mineralizers. We discover some trends in nanoplate growth that are connected to the chemical and physical properties of these RE elements. Following the order

dx.doi.org/10.1021/cm502301u | *Chem. Mater.* XXXX, XXX, XXX−XXX

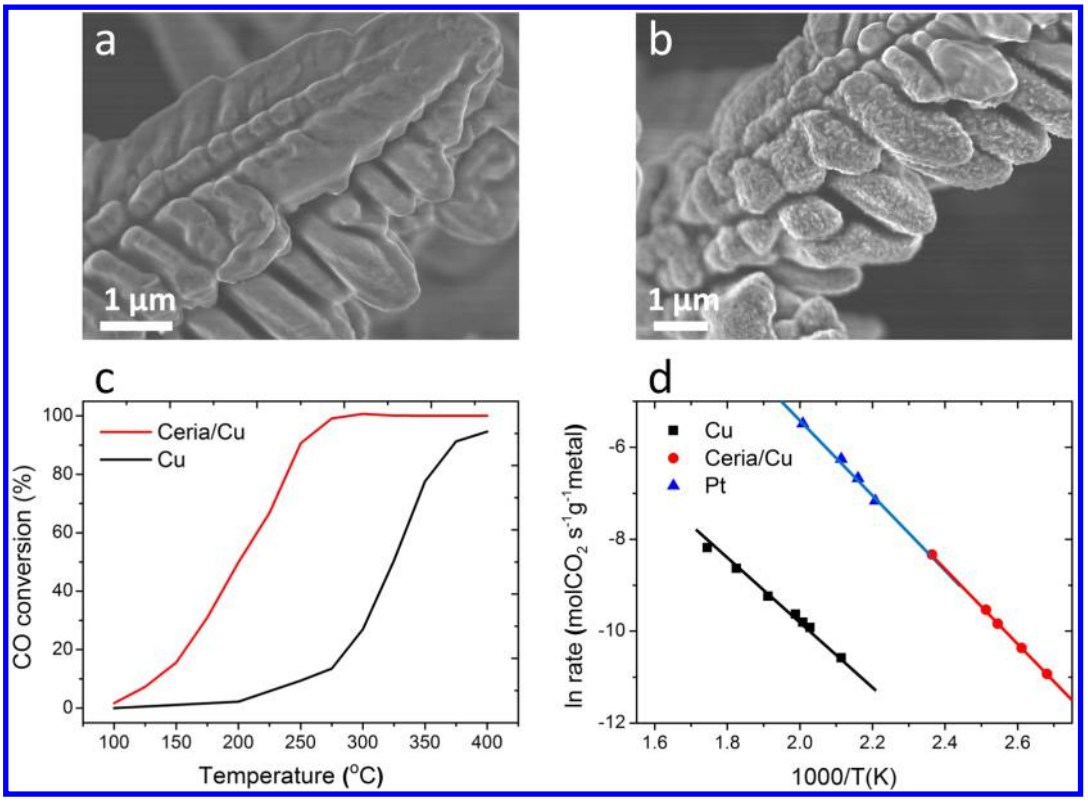

Figure 3. SEM images of (a) Cu dendrites and (b) Cu dendrites loaded with ceria nanoplates (ceria/Cu inverse catalysts); (c) the light-off curves; and (d) the Arrhenius plots for CO oxidation on Cu dendrites, ceria/Cu inverse catalysts, and Pt. Scale bars: 1 μm.

of La → Ce → Gd → Y, RE elements are classified into light and heavy RE elements, and the ionic radii decrease. According to this order, we have the following observations. (1) It is gets easier to make RE oxide nanoplates, namely, the yield increases. (2) Without a mineralizer, or with sodium diphosphate, the nanoplate growth gradually favors the round plates over the square plates: La and Ce have square nanoplates in the format of their oxides. In our synthesis, the Gd_2O_3 nanoplates are mainly round; however, observations of both round and square plates were reported.[31,40] For Y_2O_3, round nanoplates are exclusively generated, square Y_2O_3 nanoplates are neither observed in our experiments nor to our knowledge reported by other researchers. (3) The available morphologies of nanoplates get more complicated. The crystal growth habit may be responsible for the variation in nanoplate formation; however, the detailed mechanism for nanoplate growth remains to be developed. As all of these nanoplates have a cubic crystal structure, there should be no anisotropic structures: the crystal symmetries along three directions should be equivalent. In Gd_2O_3 nanoplates, Cao observed lattice fringes for (002) planes on one direction and fringes for (004) and (040) planes on the other two directions.[31] This is because symmetry breaking resulted from the ligand bonding and crystal size confinement. The same mechanism is also applicable in our case.

Because of their unique 2D structures, RE oxide nanoplates have high surface-to-volume ratios, which is highly desirable in the application of catalysis and sensing. The tunable morphologies of RE oxide nanoplates also offer suitable materials for the study of shape-dependent properties. Here, with one case on the catalysis of CO oxidation on ceria/Cu reverse catalysts, and the other case on the optics of downconversion by Eu^{3+}-doped Y_2O_3 nanophosphors, we showcase the benefit of RE oxide nanoplates in various applications.

Catalysis of CO Oxidation on Ceria/Cu Reverse Catalysts. Ceria was widely used in applications of catalysis because it shifts easily between Ce^{3+} and Ce^{4+}, which leads to a capacity to store oxygen, and it has a high population of oxygen vacancies within its structure, which leads to high oxygen mobility. Recently, inverse catalysts, oxide nanoparticles supported on metal surfaces, have received substantial attention because of their unique reactivity and selectivity as well as their ease of recycling high-cost metals that are used in catalysts.[41−43] Because of their small size and unique 2D structure, our ceria nanoplates are particularly suitable for the application of inverse catalysts. From the studies on the inverse models of well-defined surfaces, ceria on Cu has proven to have excellent activity toward CO oxidation, while ceria and Cu individually are not good catalysts for CO oxidation. Here, we prepare an inverse catalyst for CO oxidation by square ceria nanoplates (0.5%w.t.) being loaded on Cu dendrites (Figure 3a,b). As shown in Figure 3, panel c, ceria/Cu has a significantly lower light-off temperature (at least 125 °C lower) than does Cu alone for the CO oxidation reaction. In Figure 3, panel d, the Arrhenius plots are extracted from the measurements, and the apparent activation energies are calculated to be 53.21 kJ mol^{-1} for Cu dendrites, 68.34 kJ mol^{-1} for ceria/Cu inverse catalysts, and 69.01 kJ mol^{-1} for Pt catalysts. The activity of the CO oxidation on ceria/Cu inverse catalysts is comparable to that on Pt catalysts, even at a relatively low temperature. Thus, the ceria nanoplates with their unique 2D structure provide a low-cost and highly active building block for modern catalysis.

Optics of Downconversion by Eu^{3+}-Doped Y_2O_3 Nanophosphors. Y_2O_3 is one of the best host materials for optical emission and downconversion.[24,25] Because of their

dx.doi.org/10.1021/cm502301u | Chem. Mater. XXXX, XXX, XXX−XXX

quantum efficiency, which is close to 100%, Eu^{3+}-doped Y_2O_3 materials are widely used as red-emitting phosphors in lighting industry and projection television displays.[24,25] Here, we synthesize Eu^{3+}-doped Y_2O_3 nanoplates by adding 5% $Eu(Ac)_3$ in the reaction precursors. The triangle nanoplates and round nanoplates made of Eu^{3+}-doped Y_2O_3 are tested and compared to their bulk counterpart. Figure 4 shows the room temperature

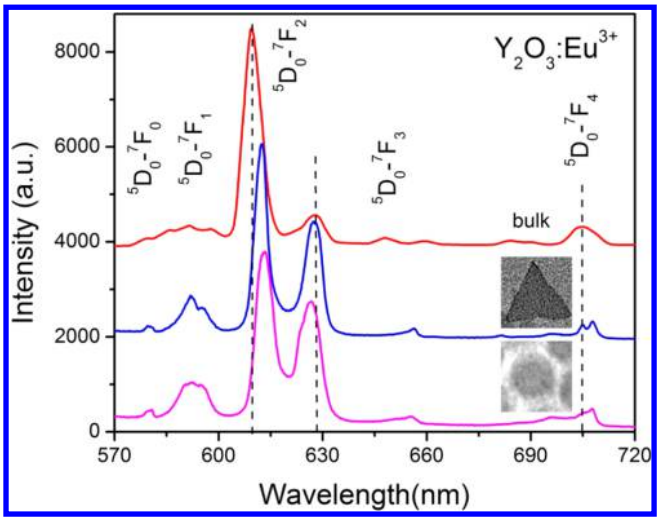

Figure 4. Luminescence spectra of Eu^{3+}-doped Y_2O_3 bulk materials (red), triangular nanoplates (blue), and round nanoplates (magenta) under 393 nm of excitation.

emission spectra of the Y_2O_3:Eu^{3+} samples under 393 nm of excitation. The emission spectrum shows narrow emissions that range from 570−720 nm, which result from the transitions from the $^5D_0$ level to the ^7F_J (J = 0, 1, 2, 3, 4) levels of Eu^{3+}. It is well-known that the electric-dipole $^5D_0 \rightarrow {}^7F_2$ transition is very sensitive to the chemical environments around the Eu^{3+} ions.[44] On the other hand, the magnetic-dipole $^5D_0 \rightarrow {}^7F_1$ transition is relatively insensitive to the symmetry of the crystal site where the Eu^{3+} ions are located. As shown in Figure 4, the $^5D_0 \rightarrow {}^7F_2$ transitions of the triangular and round nanoplates are red-shifted compared to those of the bulk phosphors, while the $^5D_0 \rightarrow {}^7F_1$ transitions of the nanoplates are more prominent.

CONCLUSION

In summary, we synthesized RE oxide (RE = La, Ce, Gd, and Y) nanoplates. We demonstrate that the use of a mineralizer in the synthesis not only boosts the yield of nanoplates, but also provides an avenue to tune the shape of nanoplates. Because of the high surface-to-volume ratios and unique surface properties, the RE oxide nanoplates can be applied in many areas. For instance, ceria/Cu inverse catalysts exhibit comparable activity to Pt toward CO oxidation, which enables an inexpensive option of catalyst in industrial chemical processes. The unique luminescence property of the Y_2O_3:Eu^{3+} nanoplate offers promising materials in the industries of lightning, display, and solar energy conversion.

METHODS

Synthesis. La_2O_3 nanoplates: 0.1 g of $La(Ac)_3$ and 0.53 g of sodium diphosphate are dissolved in a mixture of 2 mL of oleic acid (OA), 4.5 mL of oleylamine (OM), and 2 mL of 1-octadecene (ODE). The formed reaction mixture is heated to 120 °C under stirring and vacuum for 20−30 min. The reaction mixture is then heated to the reaction temperature (T) of 320 °C and is kept at 320 °C for a reaction time (t) of 60 min. After the reaction, the product mixture is allowed to cool to room temperature, followed by a wash with ethanol. The nanoplates are collected by centrifugation (6000 rpm) and are redispersed in hexane. All of the nanoplates are synthesized in a similar way, and the reaction parameters are summarized in Table 1.

Microscopic Characterizations. TEM images were taken on a JEOL1400 transmission electron micrograph at 120 kV. Scanning electron microscopy (SEM) images were taken on JEOL JSM7600F scanning electron micrograph.

Catalysis. A hexane solution of ceria nanoplates is mixed with a powder of Cu dendrites to form a ceria/Cu inverse catalyst at the loading of 0.5% wt ceria. The catalyst is then mixed with quartz at a 1:10 ratio. Before the catalytic property measurements, the catalysts are pretreated in pure O_2 at 180 °C for 30 min to remove the organic ligands that are used in the synthesis procedure. CO oxidation measurements are carried out in a flow-reactor at a gas hourly space velocity (GHSV) of 36,000 mL h^{-1} g^{-1} and are detected with a gas chromatograph (GC) equipped with a thermal conductivity detector (TCD). The gas mixture is 5 Torr CO, 2.5 Torr O_2, and He balance.

Optics. Optical measurements are performed on a Fluorolog 3 spectrometer (HORIBA Jobin Yvon) under 393 nm of excitation.

ASSOCIATED CONTENT

Supporting Information

Details for the synthesis and XRD data for the Y_2O_3 nanoplates. This material is available free of charge via the Internet at http://pubs.acs.org.

AUTHOR INFORMATION

Corresponding Author

*E-mail: cbmurray@sas.upenn.edu.

Present Addresses

[¶]Y.K., Materials Science Division, Argonne National Laboratory, Argonne, IL 60439

[‖]X.Y., Department of Chemistry, University of California at Berkeley, Berkeley, CA 94720

Table 1. Reaction Parameters for Synthesis of Nanoplates[a]

product	RE precursor	mineralizer	OA (mL)	OM (mL)	ODE (mL)	T (°C)	t (min)
Gd_2O_3 round nanoplates	0.1 g $Gd(Ac)_3$		0.2	8		360	25
Gd_2O_3 branched tripod nanoplates	0.4 g $Gd(Ac)_3$	0.17 g $NaNO_3$	1.5	1.5	7	310	40
Gd_2O_3 triangular nanoplates	0.4 g $Gd(Ac)_3$	0.17 g $NaNO_3$	1.5	2	6.5	310	40
Y_2O_3 round nanoplates	0.68 g $Y(Ac)_3$		3	3	14	310	60
Y_2O_3 tripod nanoplates	0.68 g $Y(Ac)_3$	0.34 g $NaNO_3$	2	1	17	310	30
Y_2O_3 branched tripod nanoplates	0.68 g $Y(Ac)_3$	0.34 g $NaNO_3$	3	2	15	310	30
Y_2O_3 triangular nanoplates	0.68 g $Y(Ac)_3$	0.34 g $NaNO_3$	8	8	5	310	30

[a]CeO_2 nanoplates: ceria nanoplates were synthesized as described in our previous report.[18]

dx.doi.org/10.1021/cm502301u | Chem. Mater. XXXX, XXX, XXX−XXX

Author Contributions

[⊥]These authors contributed equally.

Notes

The authors declare no competing financial interest.

■ ACKNOWLEDGMENTS

D.W. acknowledges the support of the National Natural Science Foundation of China (51062008, 21463014) and the Key Project of Chinese Ministry of Education (212095). Y.K. acknowledges the support from the National Science Foundation Grant No. MRSEC DMR11-20901, while C.B.M. and X.Y. acknowledge the support from the Office of Naval Research (ONR) Multidisciplinary University Research Initiative (MURI) on Optical Metamaterials through award N00014-10-1-0942 for the contributions to the development of the nanophosphor plates. C.B.M. thanks the Richard Perry University Professorship for the support of the supervisory role.

■ REFERENCES

(1) Murray, C. B.; Kagan, C. R.; Bawendi, M. G. *Annu. Rev. Mater. Sci.* **2000**, *30*, 545−610.
(2) Sun, S. H.; Murray, C. B.; Weller, D.; Folks, L.; Moser, A. *Science* **2000**, *287*, 1989−1992.
(3) Ahmadi, T. S.; Wang, Z. L.; Green, T. C.; Henglein, A.; El-Sayed, M. A. *Science* **1996**, *272*, 1924−1926.
(4) Mai, H. X.; Sun, L. D.; Zhang, Y. W.; Si, R.; Feng, W.; Zhang, H. P.; Liu, H. C.; Yan, C. H. *J. Phys. Chem. B* **2005**, *109*, 24380−24385.
(5) Feng, X. D.; Sayle, D. C.; Wang, Z. L.; Paras, M. S.; Santora, B.; Sutorik, A. C.; Sayle, T. X. T.; Yang, Y.; Ding, Y.; Wang, X. D.; Her, Y. S. *Science* **2006**, *312*, 1504−1508.
(6) Habas, S. E.; Lee, H.; Radmilovic, V.; Somorjai, G. A.; Yang, P. *Nat. Mater.* **2007**, *6*, 692−697.
(7) Tian, N.; Zhou, Z. Y.; Sun, S. G.; Ding, Y.; Wang, Z. L. *Science* **2007**, *316*, 732−735.
(8) Si, R.; Flytzani-Stephanopoulos, M. *Angew. Chem., Int. Ed.* **2008**, *47*, 2884−2887.
(9) Solla-Gullon, J.; Vidal-Iglesias, F. J.; Lopez-Cudero, A.; Garnier, E.; Feliu, J. M.; Aldaza, A. *Phys. Chem. Chem. Phys.* **2008**, *10*, 3689−3698.
(10) Lee, I.; Delbecq, F.; Morales, R.; Albiter, M. A.; Zaera, F. *Nat. Mater.* **2009**, *8*, 132−138.
(11) Xia, Y. N.; Xiong, Y. J.; Lim, B.; Skrabalak, S. E. *Angew. Chem., Int. Ed.* **2009**, *48*, 60−103.
(12) Kang, Y. J.; Murray, C. B. *J. Am. Chem. Soc.* **2010**, *132*, 7568−7569.
(13) Kang, Y. J.; Ye, X. C.; Murray, C. B. *Angew. Chem., Int. Ed.* **2010**, *49*, 6156−6159.
(14) Kang, Y.; Pyo, J. B.; Ye, X.; Gordon, T. R.; Murray, C. B. *ACS Nano* **2012**, *6*, 5642−5647.
(15) Kang, Y.; Li, M.; Cai, Y.; Cargnello, M.; Diaz, R. E.; Gordon, T. R.; Wieder, N. L.; Adzic, R. R.; Gorte, R. J.; Stach, E. A.; Murray, C. B. *J. Am. Chem. Soc.* **2013**, *135*, 2741−2747.
(16) Kang, Y.; Pyo, J. B.; Ye, X.; Diaz, R. E.; Gordon, T. R.; Stach, E. A.; Murray, C. B. *ACS Nano* **2013**, *7*, 645−653.
(17) Wang, C.; Daimon, H.; Lee, Y.; Kim, J.; Sun, S. *J. Am. Chem. Soc.* **2007**, *129*, 6974−6975.
(18) Wang, D. Y.; Kang, Y. J.; Doan-Nguyen, V.; Chen, J.; Kungas, R.; Wieder, N. L.; Bakhmutsky, K.; Gorte, R. J.; Murray, C. B. *Angew. Chem., Int. Ed.* **2011**, *50*, 4378−4381.
(19) Bratlie, K. M.; Lee, H.; Komvopoulos, K.; Yang, P. D.; Somorjai, G. A. *Nano Lett.* **2007**, *7*, 3097−3101.
(20) Zhang, J.; Yang, H.; Fang, J.; Zou, S. *Nano Lett.* **2010**, *10*, 638−644.
(21) Peng, X. G.; Manna, L.; Yang, W. D.; Wickham, J.; Scher, E.; Kadavanich, A.; Alivisatos, A. P. *Nature* **2000**, *404*, 59−61.
(22) Sun, Y. G.; Xia, Y. N. *Science* **2002**, *298*, 2176−2179.
(23) Ye, X.; Collins, J. E.; Kang, Y.; Chen, J.; Chen, D. T. N.; Yodh, A. G.; Murray, C. B. *Proc. Nat. Acad. Sci. U. S. A.* **2010**, *107*, 22430−22435.
(24) Schmechel, R.; Kennedy, M.; von Seggern, H.; Winkler, H.; Kolbe, M.; Fischer, R. A.; Li, X. M.; Benker, A.; Winterer, M.; Hahn, H. *J. Appl. Phys.* **2001**, *89*, 1679−1686.
(25) Dhanaraj, J.; Jagannathan, R.; Kutty, T. R. N.; Lu, C. H. *J. Phys. Chem. B* **2001**, *105*, 11098−11105.
(26) Song, Q.; Ding, Y.; Wang, Z. L.; Zhang, Z. J. *J. Phys. Chem. B* **2006**, *110*, 25547−25550.
(27) Burda, C.; Chen, X. B.; Narayanan, R.; El-Sayed, M. A. *Chem. Rev.* **2005**, *105*, 1025−1102.
(28) Yan, Z.-G.; Yan, C.-H. *J. Mater. Chem.* **2008**, *18*, 5046−5059.
(29) Trovarelli, A.; de Leitenburg, C.; Boaro, M.; Dolcetti, G. *Catal. Today* **1999**, *50*, 353−367.
(30) Wang, F.; Han, Y.; Lim, C. S.; Lu, Y. H.; Wang, J.; Xu, J.; Chen, H. Y.; Zhang, C.; Hong, M. H.; Liu, X. G. *Nature* **2010**, *463*, 1061−1065.
(31) Cao, Y. C. *J. Am. Chem. Soc.* **2004**, *126*, 7456−7457.
(32) Si, R.; Zhang, Y. W.; You, L. P.; Yan, C. H. *Angew. Chem., Int. Ed.* **2005**, *44*, 3256−3260.
(33) Xiong, Y. J.; McLellan, J. M.; Chen, J. Y.; Yin, Y. D.; Li, Z. Y.; Xia, Y. N. *J. Am. Chem. Soc.* **2005**, *127*, 17118−17127.
(34) Qin, R.; Song, H.; Pan, G.; Bai, X.; Dong, B.; Xie, S.; Liu, L.; Dai, Q.; Qu, X.; Ren, X.; Zhao, H. *Cryst. Growth Des.* **2009**, *9*, 1750−1756.
(35) Ye, X.; Chen, J.; Engel, M.; Millan, J. A.; Li, W.; Qi, L.; Xing, G.; Collins, J. E.; Kagan, C. R.; Li, J.; Glotzer, S. C.; Murray, C. B. *Nat. Chem.* **2013**, *5*, 466−473.
(36) Yu, T.; Lim, B.; Xia, Y. N. *Angew. Chem., Int. Ed.* **2010**, *49*, 4484−4487.
(37) Liang, X.; Wang, X.; Zhuang, Y.; Xu, B.; Kuang, S. M.; Li, Y. D. *J. Am. Chem. Soc.* **2008**, *130*, 2736−2737.
(38) Wang, X. D.; Summers, C. J.; Wang, Z. L. *Nano Lett.* **2004**, *4*, 423−426.
(39) Sundström, L. J. Low temperature heat capacity of the rare earth metals. In *Handbook on the Physics and Chemistry of Rare Earths, Metals*, Gschneidner, K. A., Jr., Eyring, L., Eds.; North-Holland: Amsterdam, The Netherlands, 1978; Vol. *1*, pp 379−410.
(40) Si, R.; Zhang, Y.-W.; Zhou, H.-P.; Sun, L.-D.; Yan, C.-H. *Chem. Mater.* **2007**, *19*, 18−27.
(41) Yang, F.; Graciani, J.; Evans, J.; Liu, P.; Hrbek, J.; Fdez Sanz, J.; Rodriguez, J. A. *J. Am. Chem. Soc.* **2011**, *133*, 3444−3451.
(42) Yang, F.; Choi, Y.; Agnoli, S.; Liu, P.; Stacchiola, D.; Hrbek, J.; Rodriguez, J. A. *J. Phys. Chem. C* **2011**, *115*, 23062−23066.
(43) Rodriguez, J. A.; Ma, S.; Liu, P.; Hrbek, J.; Evans, J.; Perez, M. *Science* **2007**, *318*, 1757−1760.
(44) Wei, Z. G.; Sun, L. D.; Liao, C. S.; Yan, C. H. *Appl. Phys. Lett.* **2002**, *80*, 1447−1449.